https://doi.org/10.1016/j.jpowsour.2018.08.049

Fast supercapacitors based on vertically oriented MoS₂ nanosheets on

plasma pyrolyzed cellulose filter paper

Nazifah Islam¹, Shu Wang², Juliusz Warzywoda³, Zhaoyang Fan¹*

¹Department of Electrical and Computer Engineering and Nano Tech Center, Texas Tech

University, Lubbock, TX 79409, USA

²Department of Nutritional Sciences, Texas Tech University, Lubbock, TX 79409, USA

³Materials Characterization Center, Whitacre College of Engineering, Texas Tech University,

Lubbock, TX 79409, USA

*Email: Zhaoyang.Fan@ttu.edu

ABSTRACT

Fast supercapacitors that can be charged and discharged at tens of hertz high frequency are

reported using binder-free electrodes of MoS₂ nanosheets grown on plasma pyrolyzed cellulose

microfiber (pCMF) paper. Rapid plasma pyrolysis was applied to obtain highly conductive

carbon fiber sheet from conventional cellulose filter paper to be used as a scaffold, on which

MoS₂ nanosheets were grown vertically wrapped around carbon microfibers in a hydrothermal

reaction. Such binder-free MoS₂-pCMF electrode based supercapacitor demonstrated fast-rate

performance in an aqueous electrolyte with a cutoff frequency of 103 Hz. A large specific

capacitance density of 125 mF cm⁻² was also measured. The organic electrolyte cell of these

electrodes exhibited a power density of 12.05 W cm⁻³ at a rate of 15 V s⁻¹. These MoS₂-pCMF

electrodes were highly stable. In a cycling test at a current density of 10 mA cm⁻², the cell

maintained its capacitance with trivial degradation in 50,000 cycles.

Keywords: High-frequency supercapacitor; MoS₂; nanosheet; vertical orientation; cellulose

1

1. Introduction

The fundamental merit of supercapacitors, including porous carbon based electric double layer capacitors [1, 2] and metal oxide, polymer or other compound based pseudocapacitors [3-9], is their ability to store and release large amount of energy in a relatively short time, compared to batteries. Major research efforts have been focused on enhancement of supercapacitor capacitance and energy densities. Usually, high energy density comes at a cost of slow charge-discharge rates, e.g. less than 1 Hz. Thus, developing fast and ultrafast supercapacitors that can be charged and discharged at tens to kilo hertz range has also attracted interest [10]. In particular, if high-frequency supercapacitors could be developed to efficiently respond at 120 Hz or higher frequency, they potentially can replace AC-filtering electrolytic capacitors for many power and electronics applications[11]. Currently, the reported AC-filtering supercapacitors are mostly based on a variety of carbon nanostructure electrodes, which have a limited capacitance of 1-3 mF/cm² at 120 Hz. Whether pseudocapacitive materials could be used for such high-frequency supercapacitors have not been well investigated considering that pseudocapacitive effect generally occurs at a low rate.

In recent years, transition metal dichalcogenides (TMDCs) have emerged as a potential candidate for pseudocapacitors [12, 13]. TMDCs are a family of inorganic species having 2D layered configuration, formed by one layer of transition metal elements sandwiched between two layers of chalcogens (S, Se) [12-15]. TMDCs can be semiconducting or semi-metallic depending on crystalline properties and elemental composition. Their relatively high conductivity, particularly their 2D sheet-like structures with a thickness down to the nanometer scale that offer a large available surface area, render them attractive as electrode materials for supercapacitors. Among different TMDCs that have been investigated [16-32], MoS₂ is particularly attractive with a high theoretical capacitance due to contributions from both double layer capacitance and pseudocapacitance [33, 34]. Efforts have been made to enhance the

obtainable capacitance from MoS_2 through diverse techniques. Undoubtedly, increased surface area is the most effective approach to maximize the utilization of active material. Studies revealed that whereas bulk MoS_2 can deliver mass specific capacitances of $\sim 100 \text{ F g}^{-1}$ [35-37], exfoliated or hydrothermally synthesized particulates or sheets of MoS_2 can increase the capacitance by many folds [19, 38, 39].

The focus of the studies on MoS_2 or other TMDCs as supercapacitor electrode materials is primarily set on maximizing the capacitance and energy densities. Many studies presented high gravimetric [19, 40-46], areal [17, 47, 48] and volumetric [36, 37] capacitance densities, but these high capacitances have been achieved at very low scan rates and/or low current densities. These reported cells failed to sustain their high capacitance or even work as a capacitor at scan rates above 1 V s⁻¹, suggesting they could not work at a frequency above 1 Hz.

Investigations exploiting TMDCs for high-rate or high-frequency supercapacitors have yet to be widely reported. The achievable rate performance can be significantly improved by combining MoS₂ with other conducting substances. Direct growth of MoS₂ on conducting substrates like carbon fiber [48] or metal [17, 49], as well as composites with carbon [40, 44], rGO and CNT [45, 47, 50] have been reported. In addition, metallic 1T phase MoS₂ has also been explored [37]. However, none of these structures were found to maintain the performance up to 1 V s⁻¹. On the other hand, supercapacitors at very high scan rates have been reported but with a very low capacitance density [35]. It was found in previous studies that flower- or sheet-like structures [49, 51] can achieve greater mass specific capacitance densities compared to bulk MoS₂ directly deposited on metal substrates [35-37].

In this work, we focused on achieving fast-rate supercapacitors by utilizing the excellent capacitive properties of ultrathin MoS₂ nanosheets in combination with highly conductive carbonized cellulose fibers to form binder-free freestanding electrodes. As the main

structural component of the cell walls of plants, cellulose is the most common polymer on earth, and the biomass feedstocks provide a sustainable source to extract cellulose fibers, which are an excellent precursor for producing carbon fibers. In this study, a rapid plasma pyrolysis was developed to obtain highly conductive carbon microfiber sheets, abbreviated pCMF, from the conventional filter paper. Vertically oriented MoS₂ nanosheets were grown on pCMF sheets in a hydrothermal process. MoS₂ nanosheets are vertically wrapped around each carbon fiber, thus achieving a highly conductive MoS₂-pCMF freestanding electrode structure. These nanosheets yield adequate surface area for electrode-electrolyte interface and provide rapid accessibility by ions in electrolyte, due to the vertical orientation, to achieve fast capacitive charge-discharge response. In aqueous electrolyte cells, a cutoff frequency of 103 Hz at -45° phase angle was measured. MoS₂-pCMF electrode based organic cells were also studied with a wide potential window of 2.5 V to enhance the energy and power densities. In addition to high capacitance and fast response, the stability of our MoS₂-pCMF electrode structure under continuous charge-discharge cycling operation was also demonstrated, with no obvious capacitance variation in the tested 50,000 cycles. This work is one step towards 2D TMDC based high-frequency supercapacitors.

2. Experimental section

2.1 Material preparation and characterization

Carbonized cellulose microfiber sheets were produced by rapid plasma pyrolysis technique [52], using the FisherbrandTM filter paper as a precursor, and hence are abbreviated pCMF sheets. They were prepared in a plasma-enhanced chemical vapor deposition (PECVD) reactor. Pieces of filter paper were covered with graphite sheets and placed on a Mo stage in the PECVD chamber. The chamber pressure was maintained at 30 Torr under flow of hydrogen (100 sccm) and methane (50 sccm). 1 kW microwave radiation was applied to ignite the plasma

with the samples merged in the high-temperature plasma sphere for 5 minutes. The extremely high temperature rapidly pyrolyzes the cellulose fiber sheet into carbon fiber sheet. For comparison, carbonized microfiber (CMF) sheets were also prepared by thermal pyrolysis of filter paper in Ar environment in a tube furnace [53], and this product is abbreviated aCMF sheets. Pieces of filter paper were heated to 800 °C at a rate of 4.3 K/min under Ar flow of 50 sccm. The furnace temperature was maintained at 800 °C for 2 hours, and then the product was allowed to cool down naturally.

MoS₂ nanosheets were grown on pCMF sheets in a hydrothermal reactor. 0.5 g sodium molybdate and 0.75 g thiourea were dissolved in 30 mL DI water [49, 54]. This solution and the pCMF sheets were loaded in a 45 ml Teflon cup and sealed in a stainless-steel vessel. The autoclave was heated at 220 °C for 2 hours in an electric oven, and then naturally cooled down to room temperature. After being removed from the autoclave, the samples were rinsed in DI water several times, and then they were dried in the air.

Microscopic imaging for analyzing the morphology and crystalline structure of pCMF and MoS₂-pCMF films was accomplished using a LEO SUPRA 35 scanning electron microscope (SEM) and a Hitachi H-9500 transmission electron microscope (TEM). Raman spectroscopic studies were carried out using a Bruker Optics SENTERRA dispersive Raman microscope spectrometer with an excitation laser of 532 nm, and a spectral resolution of ~ 3 –5 cm⁻¹. X-ray photoelectron spectroscopy (XPS) data were acquired using a Physical Electronics PHI 5000 VersaProbe XPS. The photoelectrons were excited by monochromatic Al K_{α} radiation (hv = 1486.6 eV), and the high-resolution spectra were acquired with a step of 0.1 eV and the pass energy of 23.5 eV. To correct for sample charging, the binding energy (BE) of spectra was referenced to the adventitious carbon C 1s BE at 284.8 eV. Thermogravimetric analyses (TGA) were performed in a Mettler Toledo TGA/SDTA851e Module. TGA

measurements were performed under air flow from room temperature to 700°C, at a ramp rate of 10 °C/min.

2.2 Supercapacitor studies

To analyze the electrode performance, 2016-type coin cells with symmetric electrodes were assembled. The performance was evaluated in 2M KCl in water and 1 M TEABF₄ in acetonitrile solutions, as aqueous and organic electrolytes, respectively. Electrochemical measurements were conducted using a Biologic SP-150 electrochemical workstation. Electrochemical impedance spectroscopy (EIS) was measured from 100 kHz to 0.1 Hz with a sinusoidal AC voltage of 10 mV amplitude. Cyclic voltammetry (CV) was carried out in the 0–0.8 V range for aqueous electrolyte cells, and the 0–2.5 V range for organic electrolyte cells. The volumetric energy and power densities were calculated based on the volume of two MoS₂-pCMF freestanding electrodes.

3. Results and Discussion

3.1 Material characterization

A photograph in Fig. 1(a) compares the filter paper before and after plasma pyrolysis, and a significant size reduction, ~ three quarters area reduction, is apparent. Cellulose polymer consists of a linear chain of ringed glucose molecules. In the high temperature plasma pyrolysis process, most of oxygen and hydrogen was lost, and cellulose was converted into amorphous carbon or graphite, resulting in the large size reduction. Microscopic morphology difference is further revealed by comparing SEM images in Fig. S1 in the Supplementary Information (SI) and Fig. 1(b). In contrast to pristine cellulose filter paper that has compact morphology with very sparse void spaces, a plasma pyrolyzed sample after a large mass loss in pyrolysis, clearly shows individual carbonized fibers and large voids of a few to tens of micrometers between them. The carbonized fibers have diameters in the few to ten micrometer range. From the low

magnification SEM image shown in Fig. 1(c), it is apparent that the growth of MoS₂ occurred uniformly all over the surface of the fibers. The morphology of the hydrothermally grown nanosheets of MoS₂ showed dependence on growth duration. Two-hour growth duration was found to produce vertical MoS₂ nanosheets uniformly wrapped around individual carbon fibers, and the height of vertical nanosheets was in the range of 100–200 nm (Fig. 1(d) and Fig. S2). For the same reactant concentration, when the hydrothermal synthesis duration was extended to 4 hrs, instead of further growth of these nanosheets to increase their height, bulky flowerlike spheres were observed to stack on the fibers (Fig. S3). We speculate that this effect arises from the re-nucleation of MoS₂ nanosheet clusters on the previously formed vertical nanosheets. Even though such a flower-like cluster morphology can increase the mass loading of MoS₂, it is not favorable for high-frequency supercapacitor electrode study in this work. Bulky flower-like spheres increase the electrode resistance and retard electrolyte ions from rapidly accessing the underlying nanosheet surface, resulting in slow charge-discharge rates. It is worth to emphasize that unlike a convention supercapacitor for energy storage that requires a high mass loading, for developing pseudocapacitive material based high-frequency supercapacitors that are capable of AC-filtering, the key is to improve their response frequency, since the achievable capacitance, even at a small mass loading, is already good enough for such an application.

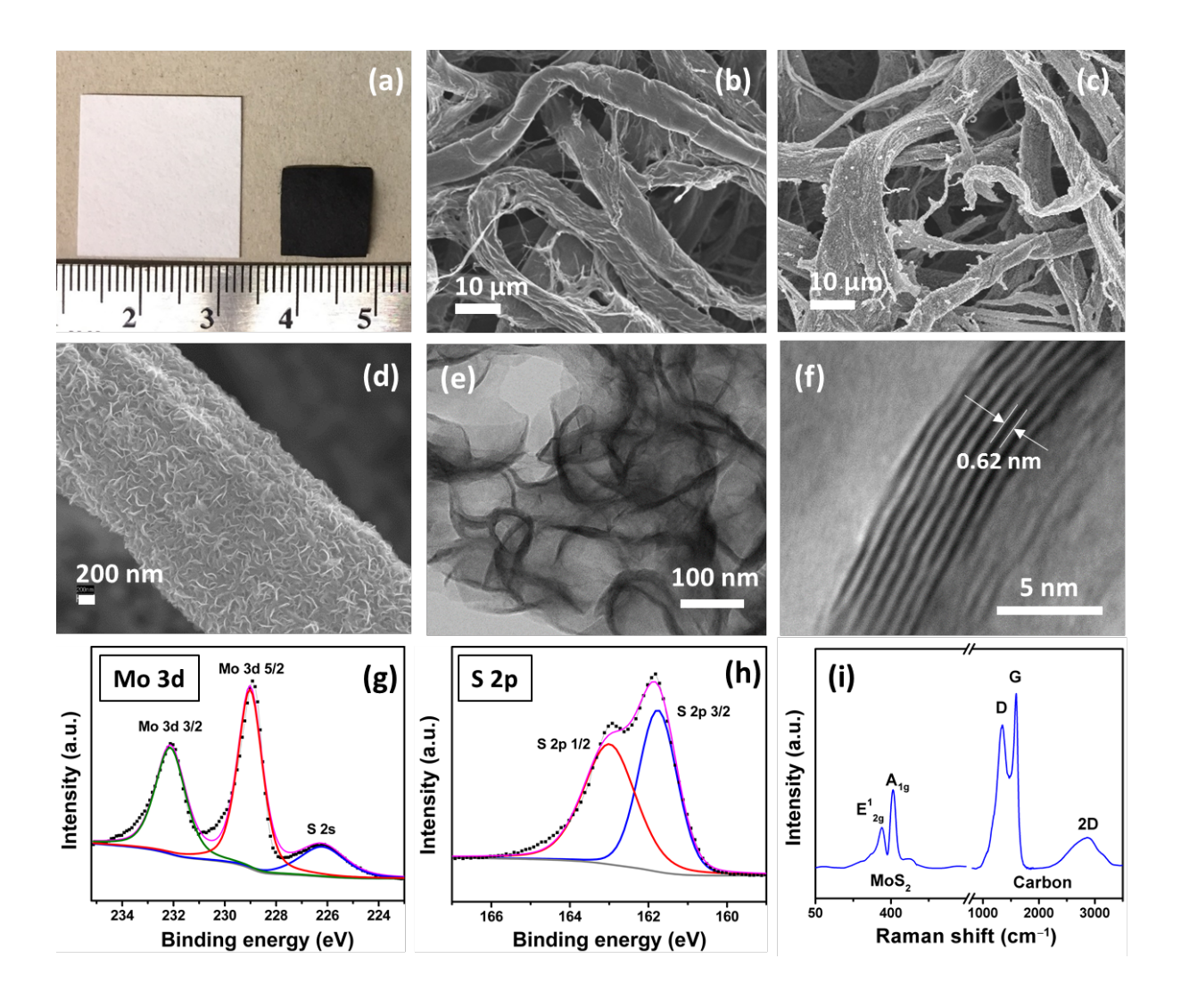


Figure 1. (a) Photographic image of a piece of cellulose filter paper before and after pyrolysis. SEM images of plasma pyrolyzed filter paper (pCMF) before (b) and after (c) MoS₂ growth. (d) High-magnification SEM image of MoS₂-pCMF sheet, showing the growth of MoS₂ through the whole sheet. Low- (e) and high- (f) resolution TEM images of MoS₂-CMF. Deconvoluted high-resolution Mo 3d (g) and S 2p (h) XPS spectra of MoS₂-pCMF. The dotted lines represent the collected spectra. (i) Raman spectrum of MoS₂-CMF.

Low- and high-resolution TEM imaging was conducted to reveal MoS₂ microscopic and layered structure. As shown in Fig. 1(e), the ultrathin MoS₂ nanosheets exhibited curled edges like rose petals. The exposed nature of the sheets is desired to obtain maximum surface

area for capacitive activity. Moreover, no bulk-like features were observed. High-resolution TEM (HRTEM) images (Figs. 1(f) and S4) revealed the layered structure of MoS2 sheets. Each sheet is formed by multiple atomic layers, and sheet thickness is in the range of few nm to a maximum ~ 10 nm. The lattice spacing between atomic layers in individual sheets was found to be 0.62 nm, which matches the characteristic d-spacing of (002) MoS2 planes. These individual sheets, being directly anchored on the carbon fiber surface, ensure fast electron transport in the whole electrode structure. The crystalline quality of the MoS2 nanosheets was further analyzed by selected area electron diffraction (SAED). The SAED pattern obtained from the nanosheets is provided in Fig. S5. The d-spacings observed in the electron diffraction pattern very closely match the X-ray diffraction (XRD) lines of the 2H phase of MoS2 (JCPDS card no. 87-2416). Thus, the crystalline state of the MoS2 sheets is predominantly 2H having trigonal prismatic coordination. In addition, the dominant lattice spacing of 0.62 nm, observed by HRTEM (Fig. 1(f)), is also confirmed by the SAED pattern, which shows the brightest ring at 0.617 nm (Fig. S5) that corresponds to (002) crystal planes.

In order to gain insight into the compositions and chemical properties of the prepared electrode materials, XPS and Raman studies were conducted. The elemental composition of the composite material, and the oxidation states of elements under consideration (i.e. C, Mo, S) are revealed by XPS. The carbon material produced by the rapid plasma pyrolysis is confirmed by the strong C 1s peak in the XPS survey spectrum of pCMF (Fig. S6). A weaker O 1s peak also appeared, likely arising from residual oxygen species in the carbon fiber or from the ambient oxygen adsorbed on the porous surface. The XPS survey spectrum of the MoS2-pCMF reveals the presence of Mo and S on the carbon surface (Fig. S6). High-resolution XPS spectra were also acquired to investigate the oxidation states of C, Mo, and S in MoS2-pCMF composite (Figs. 1(g, h) and S7). The major component at 284.8 eV of the C 1s peak indicates the dominance of C-C or C=C bonds (Fig. S7). The binding energies of Mo 3d_{5/2} (229.1 eV)

and Mo 3d_{3/2} (232.2 eV) are typical of MoS₂. The S 2s peak is present at 226.1 eV, as expected for MoS₂. The deconvolution of S 2p spectrum reveals the S 2p_{3/2} peak at 161.8 eV and S 2p_{1/2} peak at 163.0 eV, having the spin-orbit splitting ratio closer to 2:3 rather than to 1:2 ratio characteristic of elemental sulfur. This also supports the existence of S²- oxidation state [17, 38, 39, 47] in MoS₂-pCMF composite. The Raman spectrum of MoS₂-pCMF shows distinctive peaks for both MoS₂ and carbon (Fig. 1(i)). The Raman spectrum of pCMF is shown in Fig. S8 as a reference. The peaks at 376.5 cm⁻¹ and 405.5 cm⁻¹ in Fig. 1(i) correspond to the two rotational states of MoS₂: E¹_{2g} and A_{1g}, indicating in-plane and out-of-plane vibrational modes of two S atoms around the Mo atom [17, 19]. The existence of D, G and 2D peaks of carbon at 1350 cm⁻¹, 1594 cm⁻¹, and 2865 cm⁻¹, respectively (Figs. 1(i) and S8), confirms the presence of the carbonized fibers in MoS₂-pCMF.

To estimate the ratio of MoS₂ in the composite, TGA analyses were performed on powder MoS₂ and MoS₂-pCMF (2-hr duration product). As in Fig. S9, the weight loss for powder MoS₂ was 12.3%, and it was 85.6% for the composite. For both samples, the remaining yellowish solid indicated that the combustions were complete, and the residue was MoO₃. For the composite material, the first weight loss step occurring below 100°C was attributed to the loss of adhered moisture. From the weight loss patterns, the ratio of MoS₂ in the composite was calculated as 17%, with a net mass of 0.26 mg cm⁻².

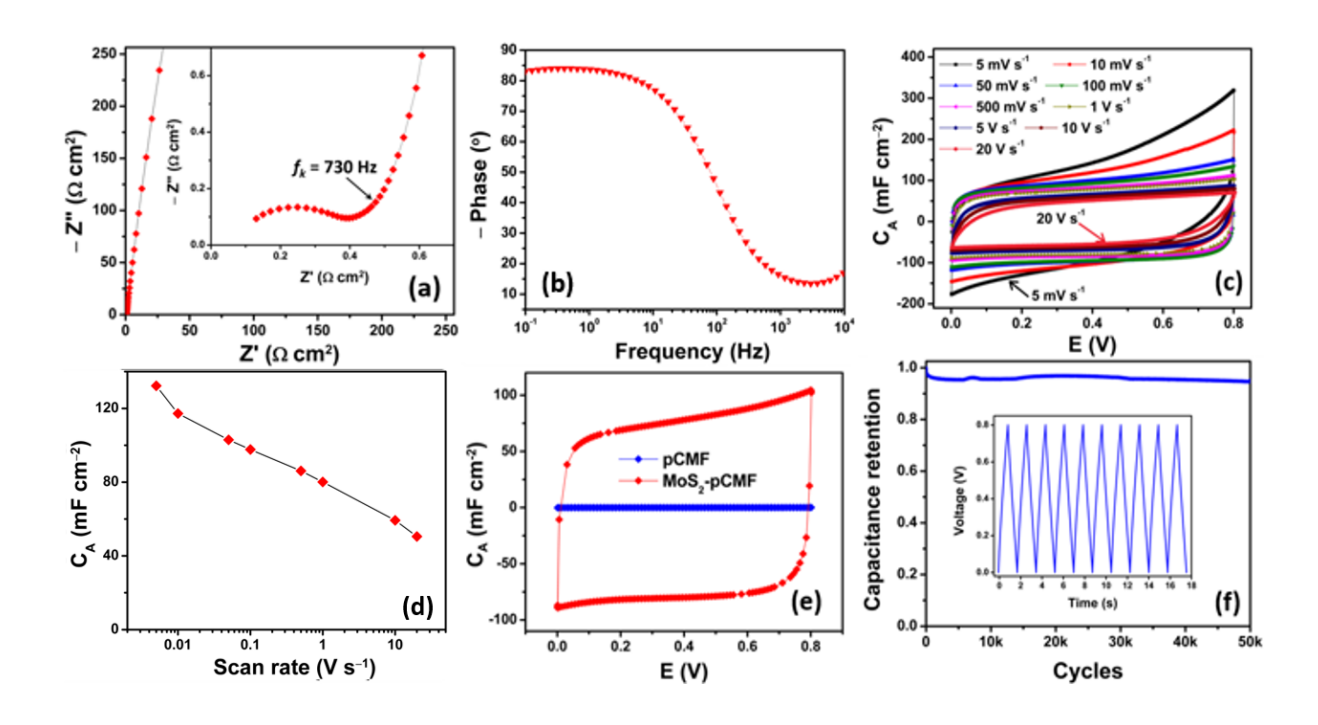


Figure 2. (a) Nyquist impedance and (b) phase spectrum of MoS₂-pCMF (2 hr growth) supercapacitor in aqueous solution. (c) Cyclic voltammetry in KCl solution from 5 mV s⁻¹ to 20 V s⁻¹. (d) Area specific capacitance versus scan rate. (e) Cyclic voltammetry at 1 V s⁻¹ for pCMF with and without MoS₂, suggesting the capacitance of pCMF scaffold is trivial. (f) Galvanostatic cycling at 10 mA cm⁻².

3.2 Supercapacitor study

3.2.1 Aqueous electrolyte cells

Electrochemical characterization of MoS₂-pCMF electrodes, including impedance spectroscopy and cyclic voltammetry, was carried out using symmetric two-electrode configuration assembled in coin cells. In aqueous electrolyte, the symmetric cell made from 2 hr duration product shows a semicircle at high frequencies (Fig. 2(a)); however, the observed semicircle width and equivalent series resistance are considerably reduced when compared to other reported TMDC electrodes [38, 45, 47, 55], and therefore a large knee frequency of 730 Hz was found. The uprightness of the impedance curve ascertains the capacitive action at lower

frequencies. The Bode phase diagram (Fig. 2(b)) is also presented. Assuming a simple RC circuit for the fast supercapacitor, which is an approximation for a frequency below the knee frequency, the Bode phase diagram shows a -45° phase angle occurring at 103 Hz, which defines the boundary between capacitance dominance and resistance dominance, and is called the cutoff frequency. It is worth mentioning that a cutoff frequency at -45° phase angle above 1 Hz is rarely observed for such redox active materials. Thus, our result is clearly an achievement, suggesting a fast charge-discharge capability of MoS2-pCMF electrodes fabricated here. The value of phase angle in Fig. 2(b), being more than 80° for frequencies up to ~ 10 Hz, suggests that the MoS₂-pCMF electrode based supercapacitor can be efficiently charged and discharged at frequencies up to 10 Hz. We attribute the high-speed response of the MoS₂-pCMF electrode to two factors. The first one is the electrode geometry with the vertically oriented MoS₂ nanosheets wrapped around the carbon microfibers in the pCMF scaffold. The large voids in the scaffold (Fig. 1(c, d)) ensure electrolyte ions freely transport around the whole 3D electrode structure, and the conductive and interconnected scaffold provides "freeway" for electron transport. Furthermore, each of the vertically oriented MoS₂ nanosheets is directly anchored on the scaffold to minimize the interface resistance facilitating electron transport, while the oriented channels between neighboring MoS₂ nanosheets (Fig. 1(e)) permit rapid access of the nanosheet surface by electrolyte ions. The second factor contributing to the fast response of the MoS₂-pCMF electrode is directly related to the unique rapid plasma pyrolysis process used to form the pCMF scaffold. For comparison, when the cellulose paper is pyrolyzed in a conventional thermal process to obtain the aCMF scaffold for MoS₂ deposition, the resulting MoS₂-aCMF electrodes have much slower response than MoS₂-pCMF electrodes. As shown in Fig. S10(a, b), a much wider semicircle feature was measured for MoS₂-aCMF electrodes in the EIS spectrum with a knee frequency of 34.5 Hz. The cutoff frequency at -45° phase angle now is only 3 Hz. We speculate that the electrode response speed

is substantially affected by the conductivity and pore properties of the carbon fiber scaffold, which depend on the pyrolysis technique. As reported previously, rapid plasma pyrolysis can dramatically enhance response speed of carbon fibers to develop kilohertz high-frequency supercapacitors [56]. This is further confirmed by directly comparing the frequency response of our bare aCMF and pCMF electrodes, as presented in Fig. S11. The pCMF electrode exhibits a cutoff frequency of 27 kHz, while it is only 1.46 kHz for aCMF. The difference in cutoff frequency, being more than one order of magnitude, confirms the superiority of pCMF over aCMF in achieving fast electron and ion transport. In addition, electronic conductivity measurements showed twofold increase in conductivity for pCMF over aCMF. The high-speed response of MoS₂-pCMF electrodes was also verified in the cyclic voltammetry study with high scan rates (Fig. 2(c)). The observed CV curves did not show deviation from rectangular behavior up to a scan rate as high as 20 V s⁻¹. This confirms the improved rate capability due to employing plasma pyrolyzed microfibers as MoS₂ deposition scaffold. The areal specific capacitance of a single electrode was derived from cyclic voltammetry data (see SI), and is plotted in Fig. 2(d). With a value of 125 mF cm⁻² at 5 mV s⁻¹ rate and 48.1 mF cm⁻² at 20 V s⁻¹ rate, the results evidently show sustenance of capacitive properties over a wide range of sweep rate for these unique MoS₂-pCMF electrodes. It should be emphasized that the measured capacitance comes exclusively from MoS₂ nanoflakes with no contribution from the underlying carbon fiber surface, considering that the scaffold surface is completely covered with MoS₂. In fact, a bare pCMF scaffold itself does not provide a meaningful capacitance when compared to MoS₂ nanoflakes, as shown in Fig. 2(e).

Admittedly, the fast supercapacitor cells based on MoS_2 -pCMF electrodes have lower capacitance than those reported in the literature that only run at low speed [2, 16, 17, 19, 37]. Thus, for comparison, CV of cells based on MoS_2 -aCMF electrodes was also studied at low scan rates from 10 mV s⁻¹ to 1 V s⁻¹ (Fig. S10 (c)), and the derived capacitance versus scan rate

is presented in Fig. S10 (d). The area specific capacitance was 183 mF cm⁻² at 10 mV s⁻¹ and 113 mF cm⁻² at 1 V s⁻¹, indicating preserved charge storage capability over a wide rate range. At higher rates (Fig. S10 (e)), the CV profile significantly deviate from a rectangle, suggesting it could not respond very well at such high rates.

A distinctive feature observed from the CV study of MoS₂-pCMF based cells is the rectangular shape of the curves throughout the investigated scan rate range. It is known that sheet-like structures of MoS₂ are capable of both pseudocapacitive and double layer actions [33, 34]. In our study, the electrodes clearly demonstrate the double layer-like rectangular plots, confirming that the charge storage mechanism is dominated by double layer and/or surface redox reactions, and the absence of peaks over the voltage window suggests absence of intercalation. The high area specific capacitance is a direct consequence of employing a 3D microfiber network scaffold instead of a flat substrate. Moreover, it has been pointed out in many relevant studies that the achievable capacitance from MoS₂ largely depends on the efficiency of electron transfer between the substrate and the MoS₂ nanostructures [17, 47]. The high gravimetric capacitance density confirms the effective utilization of the active MoS₂ material grown on the carbonized microfibers. The fact that the nanosheets are only a few nm thick and the individual sheets are directly grown on the carbon fibers, maximizes the available surface area for capacitive action and minimizes the resistance between the active material and the conductive support. In addition, the voids between sheets facilitate efficient ion transport. All these factors effectively result in the extraordinary capacitance retention over a large scan speed range. Such retention of high capacitance over more than 3 orders of magnitude increase of scan rate is a prominent feature of these MoS₂-CMF electrodes, and has been rarely observed for TMDC based supercapacitors.

Another characteristic parameter of supercapacitors is their cycling stability, particularly for the pseudocapacitive electrodes. Galvanostatic charge-discharge tests of our

MoS₂-pCMF electrode based cells were conducted under a high current density of 10 mA cm² in KCl aqueous electrolyte. The electrode capacitance retention is shown in Fig. 2(f). The capacitance initially experienced slight decrease during the first few hundred cycles, probably due to surface-related reactions. Afterwards, it stabilized and remained almost constant over the rest of the cycling duration. After 50,000 fully charging-discharging cycles, the capacitance retention was 94.65% of the initial value. It is noted that most studies on MoS₂ electrodes reported capacitance retention for typically up to few thousand cycles and rarely used more than 10,000 cycles [19, 35, 47]. The outstanding cycling stability of our MoS₂-pCMF freestanding electrodes confirms the chemical and structural stability of MoS₂ nanosheets and pCMF scaffold, as well as the strong bonding between them.

3.2.2 Organic electrolyte cells

We further applied these MoS₂ based electrodes in organic electrolyte to enhance the energy density. To achieve a high energy density, high voltage window is necessary along with high capacitance density. Compared to aqueous electrolytes, organic solvent-based electrolytes inherently possess a much wider potential window, which is defined by dissociation potential of liquid solvents. Typically, the functional potential range for aqueous electrolytes is limited below 0.8 V, while organic electrolytes can function up to at least 2.5 V. The impedance characteristic of MoS₂-pCMF in organic electrolyte composed of 1M TEABF₄, dissolved in anhydrous acetonitrile medium, is presented in Fig. 3(a, b). In contrast to the same electrode used in the aqueous KCl electrolyte (Fig. 2(a, b)), the organic cell exhibits a much larger semicircle feature with a smaller knee frequency of 141 Hz. A cutoff frequency of ~16 Hz was measured, suggesting a more sluggish electron transfer on the electrode and a lower ion transport rate in the organic electrolyte. This is not surprising since organic electrolytes generally have much lower ionic conductivity. The CV curves at scan rates from 0.1 to 20 V s⁻¹ in a voltage range of 0-2.5 V are presented in Fig. 3(c). Capacitance densities of 47.7 mF cm⁻², 34.1

mF cm⁻², 26.8 mF cm⁻², 19.3 mF cm⁻² and 15.9 mF cm⁻² were obtained at 10 mV s⁻¹, 100 mV s⁻¹, 1 V s⁻¹, 10 V s⁻¹ and 20V s⁻¹, respectively (Fig. 3(d)).

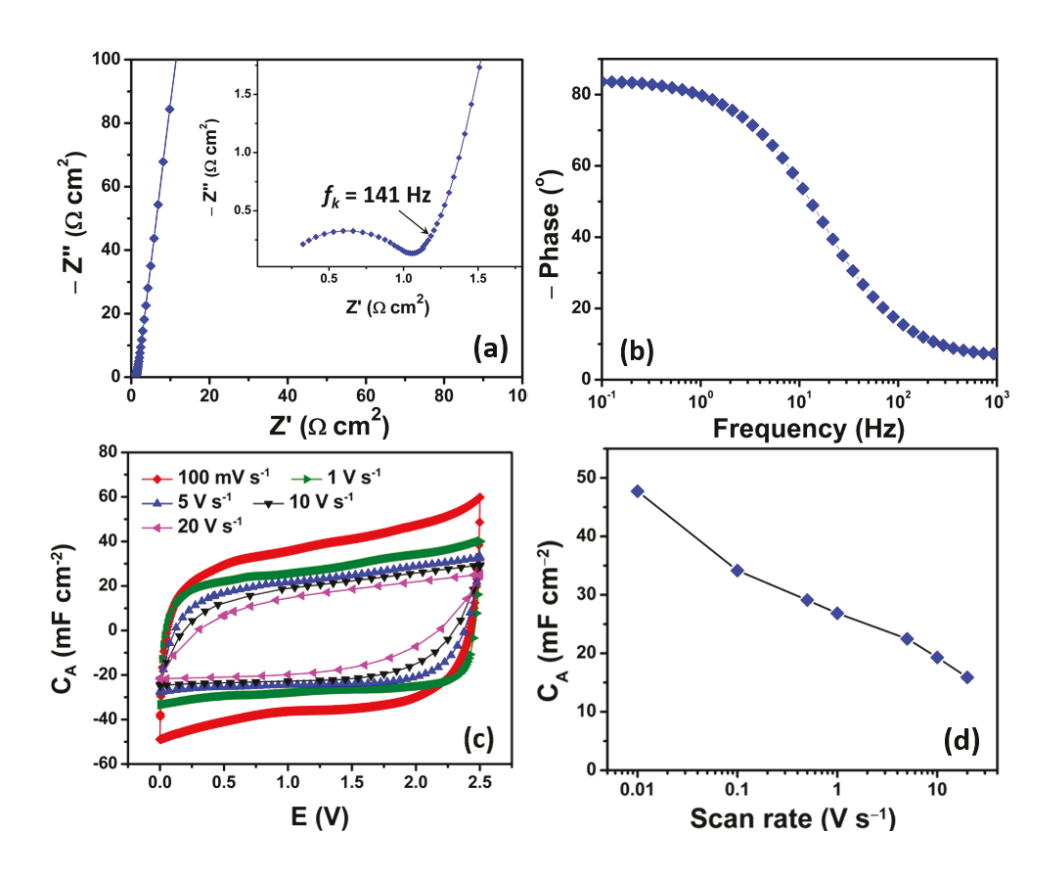


Figure 3. (a) Nyquist and (b) Bode phase spectra of MoS₂-pCMF capacitors in organic (1M TEABF₄/Acetonitrile) electrolyte. (c) Cyclic voltammograms from MoS₂-pCMF based capacitors in organic electrolyte at scan rates from 100 mV s⁻¹ to 20 V s⁻¹. (d) Capacitance versus scan rate for MoS₂-pCMF electrodes in organic electrolyte.

Even though these organic cells have a smaller cutoff frequency than the aqueous cells, their speed is still much higher than other reported aqueous cells. Therefore, we expect our cells could achieve both high energy and high power density, particularly considering that the freestanding electrodes we used have a small volume. Energy and power densities based on the cyclic voltammetry data were calculated (see SI). The maximum energy density of 2.08 mWh

cm⁻³ was obtained using organic electrolyte cell at 10 mV s⁻¹, and the maximum power density of 12.05 W cm⁻³ was also achieved for the same cell at 15 V s⁻¹. Power densities of 21.63 W cm⁻³ at 10 Hz and 5.28 W cm⁻³ at 1 Hz were calculated (see SI), with the corresponding energy densities being 0.6 mWh cm⁻³ and 0.73 mWh cm⁻³, respectively. When compared to volume specific energy and power densities of commercial supercapacitors (activated carbon based) and electrolytic capacitors, our MoS₂ based supercapacitors possess energy densities in the range similar to activated carbon supercapacitors, but their power density is in the range of fast electrolytic capacitors (1-100 W cm⁻³) [33, 37]. The carbon based EDLC supercapacitors cannot efficiently response above 1 Hz for fast rate applications, and the electrolytic capacitors' energy density is in the range of μ Wh cm⁻³, too small to be considered as a storage element. The energy and power densities calculated here imply that the MoS₂-pCMF based supercapacitors are capable of operating in practical cases where high energy storage and rapid release are needed.

Conclusions

In this work, fast supercapacitors with high power and high energy densities are reported by exploiting the excellent capacitive properties of ultrathin MoS₂ nanosheets in combination with highly conductive carbonized cellulose fibers that were used to form binder-free electrodes. A rapid plasma pyrolysis was developed to convert filter paper into highly conductive carbon microfiber sheets, on which vertically oriented MoS₂ nanosheets were grown hydrothermally, thus producing a highly conductive MoS₂-pCMF freestanding electrode structure. These nanosheets yield adequate surface area for electrode-electrolyte interface, and provide rapid accessibility of electrolyte for fast capacitive charge-discharge response. A cutoff frequency of 103 Hz at –45° phase angle was measured in aqueous electrolyte cells. MoS₂-pCMF electrode based organic cells were also studied with a wide potential window to enhance

the energy and power densities. In addition to high capacitance and fast response, the stability of our electrode structure under continuous charge-discharge operation was demonstrated, with no obvious capacitance variation in the tested 50,000 cycles. Such a supercapacitor is potentially suitable for applications where storage and release of ultra-high amount of energy is required within sub-second. Our results indicate that although this MoS₂-pCMF electrode-based cell is still incapable of acting as AC-filtering capacitor, further work such as tailoring the conductivity and mass loading of TMD nanosheets might be able to further improve their frequency response.

Acknowledgements: This work was supported by National Science Foundation (1611060).

REFERENCES

- [1] L. Qie, W. Chen, H. Xu, X. Xiong, Y. Jiang, F. Zou, X. Hu, Y. Xin, Z. Zhang, Y. Huang, Synthesis of functionalized 3D hierarchical porous carbon for high-performance supercapacitors, Energy & Environmental Science, 6 (2013) 2497-2504.
- [2] L.-F. Chen, X.-D. Zhang, H.-W. Liang, M. Kong, Q.-F. Guan, P. Chen, Z.-Y. Wu, S.-H. Yu, Synthesis of Nitrogen-Doped Porous Carbon Nanofibers as an Efficient Electrode Material for Supercapacitors, ACS Nano, 6 (2012) 7092-7102.
- [3] X. Pan, Y. Zhao, G. Ren, Z. Fan, Highly conductive VO2 treated with hydrogen for supercapacitors, Chem Commun (Camb), 49 (2013) 3943-3945.
- [4] X. Pan, G.F. Ren, M.N.F. Hoque, S. Bayne, K. Zhu, Z.Y. Fan, Fast Supercapacitors Based on Graphene-Bridged V2O3/VOx Core-Shell Nanostructure Electrodes with a Power Density of 1 MW kg(-1), Adv Mater Interfaces, 1 (2014).
- [5] F. Zhuangjun, Y. Jun, W. Tong, Z. Linjie, N. Guoqing, L. Tianyou, W. Fei, Asymmetric Supercapacitors Based on Graphene/MnO2 and Activated Carbon Nanofiber Electrodes with High Power and Energy Density, Advanced Functional Materials, 21 (2011) 2366-2375.
- [6] C.-C. Hu, K.-H. Chang, M.-C. Lin, Y.-T. Wu, Design and Tailoring of the Nanotubular Arrayed Architecture of Hydrous RuO2 for Next Generation Supercapacitors, Nano Letters, 6 (2006) 2690-2695.
- [7] X. Xiong, G. Waller, D. Ding, D. Chen, B. Rainwater, B. Zhao, Z. Wang, M. Liu, Controlled synthesis of NiCo2S4 nanostructured arrays on carbon fiber paper for high-performance pseudocapacitors, Nano Energy, 16 (2015) 71-80.
- [8] X. Xiong, C. Yang, G. Wang, Y. Lin, X. Ou, J.-H. Wang, B. Zhao, M. Liu, Z. Lin, K. Huang, SnS nanoparticles electrostatically anchored on three-dimensional N-doped graphene as an active and durable anode for sodium-ion batteries, Energy & Environmental Science, 10 (2017) 1757-1763.
- [9] X. Xiong, D. Ding, D. Chen, G. Waller, Y. Bu, Z. Wang, M. Liu, Three-dimensional ultrathin Ni(OH)2 nanosheets grown on nickel foam for high-performance supercapacitors, Nano Energy, 11 (2015) 154-161.
- [10] Z. Fan, N. Islam, S.B. Bayne, Towards kilohertz electrochemical capacitors for filtering and pulse energy harvesting, Nano Energy, 39 (2017) 306-320.

- [11] J.R. Miller, R.A. Outlaw, B.C. Holloway, Graphene double-layer capacitor with ac line-filtering performance, Science, 329 (2010) 1637-1639.
- [12] X. Chia, A.Y.S. Eng, A. Ambrosi, S.M. Tan, M. Pumera, Electrochemistry of Nanostructured Layered Transition-Metal Dichalcogenides, Chem Rev, 115 (2015) 11941-11966.
- [13] H. Wang, H.B. Feng, J.H. Li, Graphene and Graphene-like Layered Transition Metal Dichalcogenides in Energy Conversion and Storage, Small, 10 (2014) 2165-2181.
- [14] M. Pumera, Z. Sofer, A. Ambrosi, Layered transition metal dichalcogenides for electrochemical energy generation and storage, J Mater Chem A, 2 (2014) 8981-8987.
- [15] W. Choi, N. Choudhary, G.H. Han, J. Park, D. Akinwande, Y.H. Lee, Recent development of two-dimensional transition metal dichalcogenides and their applications, Materials Today, 20 (2017) 116-130
- [16] M.A. Bissett, I.A. Kinloch, R.A.W. Dryfe, Characterization of MoS2–Graphene Composites for High-Performance Coin Cell Supercapacitors, Acs Appl Mater Inter, 7 (2015) 17388-17398.
- [17] D.K. Nandi, S. Sahoo, S. Sinha, S. Yeo, H. Kim, R.N. Bulakhe, J. Heo, J.-J. Shim, S.-H. Kim, Highly Uniform Atomic Layer-Deposited MoS2@3D-Ni-Foam: A Novel Approach To Prepare an Electrode for Supercapacitors, Acs Appl Mater Inter, 9 (2017) 40252-40264.
- [18] A. Winchester, S. Ghosh, S. Feng, A.L. Elias, T. Mallouk, M. Terrones, S. Talapatra, Electrochemical Characterization of Liquid Phase Exfoliated Two-Dimensional Layers of Molybdenum Disulfide, Acs Appl Mater Inter, 6 (2014) 2125-2130.
- [19] A. Gigot, M. Fontana, M. Serrapede, M. Castellino, S. Bianco, M. Armandi, B. Bonelli, C.F. Pirri, E. Tresso, P. Rivolo, Mixed 1T-2H Phase MoS2/Reduced Graphene Oxide as Active Electrode for Enhanced Supercapacitive Performance, ACS Applied Materials and Interfaces, 8 (2016) 32842-32852.
- [20] E.G.D. Firmiano, A.C. Rabelo, C.J. Dalmaschio, A.N. Pinheiro, E.C. Pereira, W.H. Schreiner, E.R. Leite, Supercapacitor Electrodes Obtained by Directly Bonding 2D MoS 2 on Reduced Graphene Oxide, Adv Energy Mater, 4 (2014).
- [21] S. Liu, Y. Zeng, M. Zhang, S. Xie, Y. Tong, F. Cheng, X. Lu, Binder-free WS2 nanosheets with enhanced crystallinity as a stable negative electrode for flexible asymmetric supercapacitors, J Mater Chem A, 5 (2017) 21460-21466.
- [22] L. Tsung-Wu, S. Thangarasu, W. Ai-Yin, C. Ting-Yu, L. Jeng-Yu, S. Li–Dong, Ternary Composite Nanosheets with MoS2/WS2/Graphene Heterostructures as High-Performance Cathode Materials for Supercapacitors, Chemelectrochem, 5 (2018) 1024-1031.
- [23] S. Ratha, C.S. Rout, Supercapacitor Electrodes Based on Layered Tungsten Disulfide-Reduced Graphene Oxide Hybrids Synthesized by a Facile Hydrothermal Method, Acs Appl Mater Inter, 5 (2013) 11427-11433.
- [24] T.M. Masikhwa, F. Barzegar, J.K. Dangbegnon, A. Bello, M.J. Madito, D. Momodu, N. Manyala, Asymmetric supercapacitor based on VS2 nanosheets and activated carbon materials, Rsc Adv, 6 (2016) 38990-39000.
- [25] J. Feng, X. Sun, C. Wu, L. Peng, C. Lin, S. Hu, J. Yang, Y. Xie, Metallic Few-Layered VS2 Ultrathin Nanosheets: High Two-Dimensional Conductivity for In-Plane Supercapacitors, J Am Chem Soc, 133 (2011) 17832-17838.
- [26] S.K. Balasingam, J.S. Lee, Y. Jun, Few-layered MoSe2 nanosheets as an advanced electrode material for supercapacitors, Dalton T, 44 (2015) 15491-15498.
- [27] S. Jianfeng, W. Jingjie, P. Liyuan, R.M.T. F., Z. ZhuQing, Z. Fangfang, Z. Xiang, A.P. M., Y. Mingxin, CoNi2S4-Graphene-2D-MoSe2 as an Advanced Electrode Material for Supercapacitors, Adv Energy Mater, 6 (2016) 1600341.
- [28] K.-J. Huang, J.-Z. Zhang, Y. Fan, Preparation of layered MoSe2 nanosheets on Ni-foam substrate with enhanced supercapacitor performance, Mater Lett, 152 (2015) 244-247.
- [29] H. Peng, J. Zhou, K. Sun, G. Ma, Z. Zhang, E. Feng, Z. Lei, High-Performance Asymmetric Supercapacitor Designed with a Novel NiSe@MoSe2 Nanosheet Array and Nitrogen-Doped Carbon Nanosheet, ACS Sustainable Chemistry & Engineering, 5 (2017) 5951-5963.
- [30] D. Chakravarty, D.J. Late, Microwave and hydrothermal syntheses of WSe2 micro/nanorods and their application in supercapacitors, Rsc Adv, 5 (2015) 21700-21709.

- [31] D.A. Nguyen, H.M. Oh, N.T. Duong, S. Bang, S.J. Yoon, M.S. Jeong, Highly Enhanced Photoresponsivity of a Monolayer WSe2 Photodetector with Nitrogen-Doped Graphene Quantum Dots, Acs Appl Mater Inter, 10 (2018) 10322-10329.
- [32] A. Ali, W.-C. Oh, Preparation of Nanowire like WSe2-Graphene Nanocomposite for Photocatalytic Reduction of CO2 into CH3OH with the Presence of Sacrificial Agents, Sci Rep-Uk, 7 (2017) 1867.
- [33] G. Sun, X. Zhang, R. Lin, J. Yang, H. Zhang, P. Chen, Hybrid Fibers Made of Molybdenum Disulfide, Reduced Graphene Oxide, and Multi-Walled Carbon Nanotubes for Solid-State, Flexible, Asymmetric Supercapacitors, Angewandte Chemie International Edition, 54 (2015) 4651-4656. [34] J.M. Soon, K.P. Loh, Electrochemical double-layer capacitance of MoS2 nanowall films, Electrochem Solid St, 10 (2007) A250-A254.
- [35] Y. Yang, H.L. Fei, G.D. Ruan, C.S. Xiang, J.M. Tour, Edge-Oriented MoS2 Nanoporous Films as Flexible Electrodes for Hydrogen Evolution Reactions and Supercapacitor Devices, Adv Mater, 26 (2014) 8163-8168.
- [36] N. Choudhary, M. Patel, Y.H. Ho, N.B. Dahotre, W. Lee, J.Y. Hwang, W. Choi, Directly deposited MoS2 thin film electrodes for high performance supercapacitors, J Mater Chem A, 3 (2015) 24049-24054.
- [37] M. Acerce, D. Voiry, M. Chhowalla, Metallic 1T phase MoS2 nanosheets as supercapacitor electrode materials, Nat Nanotechnol, 10 (2015) 313-318.
- [38] T. Sun, Z. Li, X. Liu, L. Ma, J. Wang, S. Yang, Facile construction of 3D graphene/MoS2 composites as advanced electrode materials for supercapacitors, J Power Sources, 331 (2016) 180-188.
- [39] Y. Jia, H. Wan, L. Chen, H. Zhou, J. Chen, Hierarchical nanosheet-based MoS2/graphene nanobelts with high electrochemical energy storage performance, J Power Sources, 354 (2017) 1-9. [40] K.J. Huang, L. Wang, J.Z. Zhang, K. Xing, Synthesis of molybdenum disulfide/carbon aerogel composites for supercapacitors electrode material application, J Electroanal Chem, 752 (2015) 33-40. [41] M.S. Javed, S. Dai, M. Wang, D. Guo, L. Chen, X. Wang, C. Hu, Y. Xi, High performance solid.
- [41] M.S. Javed, S. Dai, M. Wang, D. Guo, L. Chen, X. Wang, C. Hu, Y. Xi, High performance solid state flexible supercapacitor based on molybdenum sulfide hierarchical nanospheres, J Power Sources, 285 (2015) 63-69.
- [42] K.C. Pham, D.S. McPhail, A.T.S. Wee, D.H.C. Chua, Amorphous molybdenum sulfide on graphene-carbon nanotube hybrids as supercapacitor electrode materials, Rsc Adv, 7 (2017) 6856-6864.
- [43] S.K. Balasingam, M. Lee, B.H. Kim, J.S. Lee, Y. Jun, Freeze-dried MoS2 sponge electrodes for enhanced electrochemical energy storage, Dalton T, 46 (2017) 2122-2128.
- [44] L.-Q. Fan, G.-J. Liu, C.-Y. Zhang, J.-H. Wu, Y.-L. Wei, Facile one-step hydrothermal preparation of molybdenum disulfide/carbon composite for use in supercapacitor, Int J Hydrogen Energ, 40 (2015) 10150-10157.
- [45] B. Xie, Y. Chen, M. Yu, T. Sun, L. Lu, T. Xie, Y. Zhang, Y. Wu, Hydrothermal synthesis of layered molybdenum sulfide/N-doped graphene hybrid with enhanced supercapacitor performance, Carbon, 99 (2016) 35-42.
- [46] C. Sha, B. Lu, H. Mao, J. Cheng, X. Pan, J. Lu, Z. Ye, 3D ternary nanocomposites of molybdenum disulfide/polyaniline/reduced graphene oxide aerogel for high performance supercapacitors, Carbon, 99 (2016) 26-34.
- [47] S. Wang, J. Zhu, Y. Shao, W. Li, Y. Wu, L. Zhang, X. Hao, Three-Dimensional MoS2 @CNT/RGO Network Composites for High-Performance Flexible Supercapacitors, Chemistry, (2017).
- [48] S.K. Balasingam, A. Thirumurugan, J.S. Lee, Y. Jun, Amorphous MoSx thin-film-coated carbon fiber paper as a 3D electrode for long cycle life symmetric supercapacitors, Nanoscale, 8 (2016) 11787-11791.
- [49] L. Wang, Y. Ma, M. Yang, Y. Qi, Titanium plate supported MoS2 nanosheet arrays for supercapacitor application, Appl Surf Sci, 396 (2017) 1466-1471.
- [50] R.N. Bulakhe, V.H. Nguyen, J.J. Shim, Layer-structured nanohybrid MoS2@rGO on 3D nickel foam for high performance energy storage applications, New J Chem, 41 (2017) 1473-1482.
- [51] X.P. Zhou, B. Xu, Z.F. Lin, D. Shu, L. Ma, Hydrothermal Synthesis of Flower-Like MoS2 Nanospheres for Electrochemical Supercapacitors, J Nanosci Nanotechno, 14 (2014) 7250-7254.

- [52] N. Islam, S. Li, G. Ren, Y. Zu, J. Warzywoda, S. Wang, Z. Fan, High-frequency electrochemical capacitors based on plasma pyrolyzed bacterial cellulose aerogel for current ripple filtering and pulse energy storage, Nano Energy, 40 (2017) 107-114.
- [53] S. Li, G. Ren, M.N.F. Hoque, Z. Dong, J. Warzywoda, Z. Fan, Carbonized cellulose paper as an effective interlayer in lithium-sulfur batteries, Appl Surf Sci, 396 (2017) 637-643.
- [54] H. Miao, X. Hu, Q. Sun, Y. Hao, H. Wu, D. Zhang, J. Bai, E. Liu, J. Fan, X. Hou, Hydrothermal synthesis of MoS2 nanosheets films: Microstructure and formation mechanism research, Mater Lett, 166 (2016) 121-124.
- [55] R. Zhou, C.-j. Han, X.-m. Wang, Hierarchical MoS2-coated three-dimensional graphene network for enhanced supercapacitor performances, J Power Sources, 352 (2017) 99-110.
- [56] N. Islam, M.N. Ferdous Hoque, Y. Zu, S. Wang, Z. Fan, Carbon Nanofiber Aerogel Converted from Bacterial Cellulose for Kilohertz AC-Supercapacitors, MRS Advances, (2018) 1-6.

Supplementary Information

Fast supercapacitors based on vertically oriented MoS₂ nanosheets on plasma pyrolyzed cellulose fiber paper

Nazifah Islam¹, Shu Wang², Juliusz Warzywoda³, Zhaoyang Fan¹*

¹Department of Electrical and Computer Engineering and Nano Tech Center, Texas Tech University, Lubbock, TX 79409, USA

²Department of Nutritional Sciences, Texas Tech University, Lubbock, TX 79409, USA

³Materials Characterization Center, Whitacre College of Engineering, Texas Tech University, Lubbock, TX 79409, USA

*Email: Zhaoyang.Fan@ttu.edu

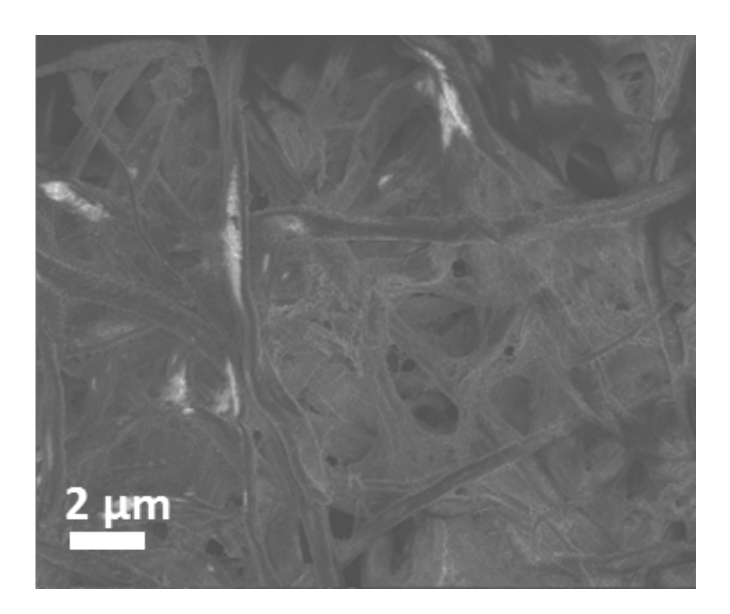


Fig. S1. SEM image of pristine cellulose filter paper, showing a compact morphology with very sparse void spaces between cellulose fibers.

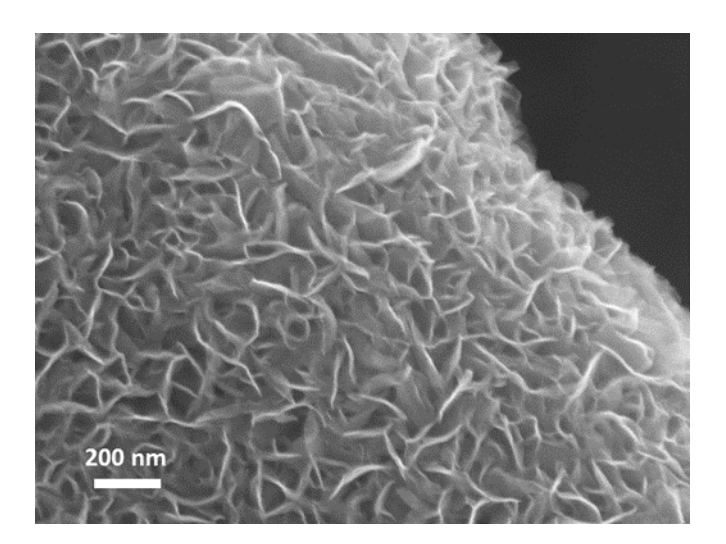


Fig. S2. High-magnification SEM image of MoS₂-pCMF after two-hour hydrothermal growth, showing vertical MoS₂ nanosheets deposition around the surface of a carbonized fiber.

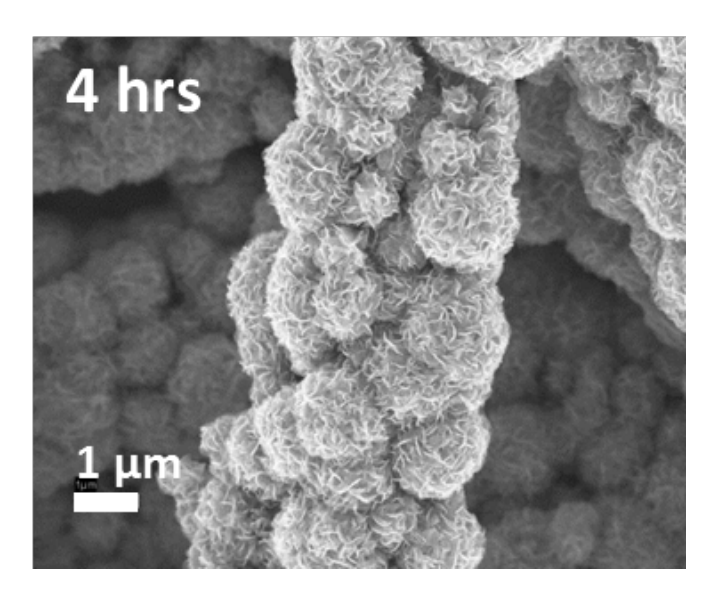


Fig. S3. SEM image of MoS₂-pCMF after four-hour hydrothermal growth, showing bulky flower-like spheres stacked on the individual carbon fibers.

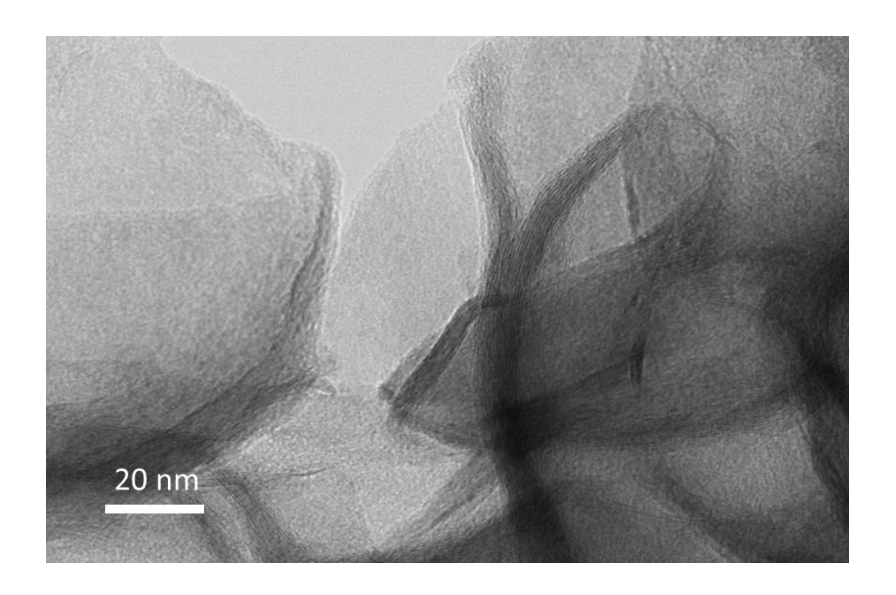


Fig. S4. High-resolution TEM image of MoS_2 nanosheets.

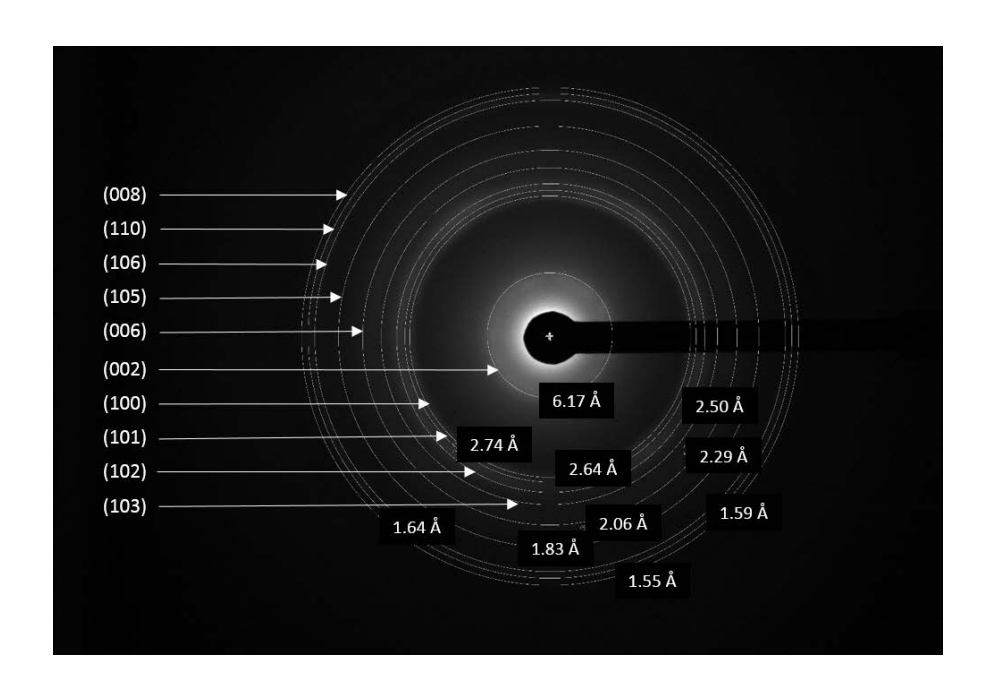


Fig. S5. Selected area electron diffraction (SAED) pattern of MoS₂ nanosheets, showing the d-spacings and the corresponding lattice planes of the 2H phase of MoS₂ (JCPDS card no. 87-2416).

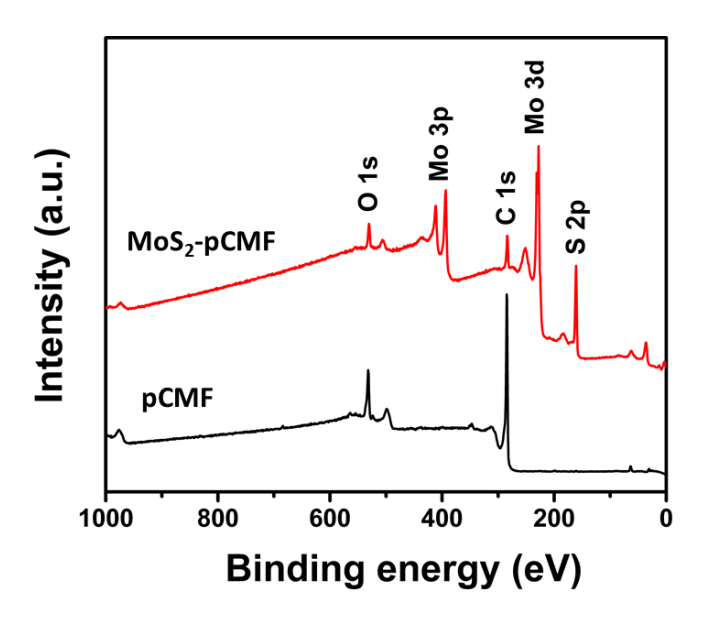


Fig. S6. XPS survey spectra of carbonized fibers pCMF and MoS₂-pCMF composite.

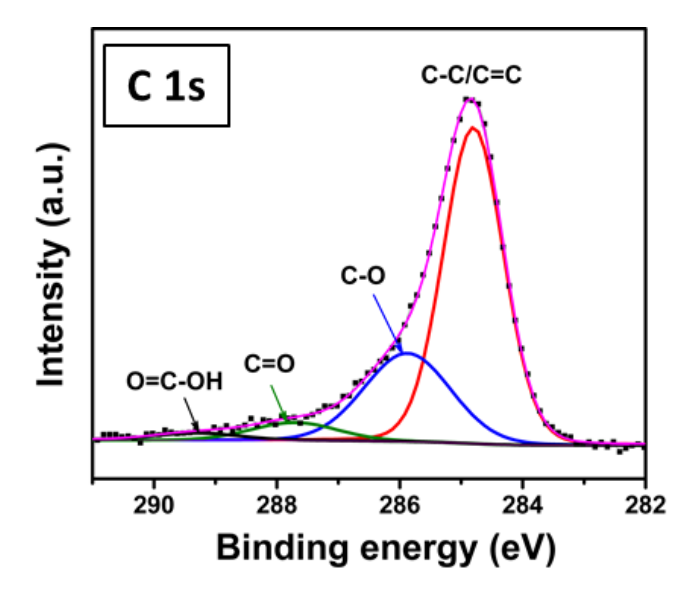


Fig. S7. High-resolution C1s XPS spectrum of MoS₂-pCMFand its deconvolution, showing different chemical bonds.

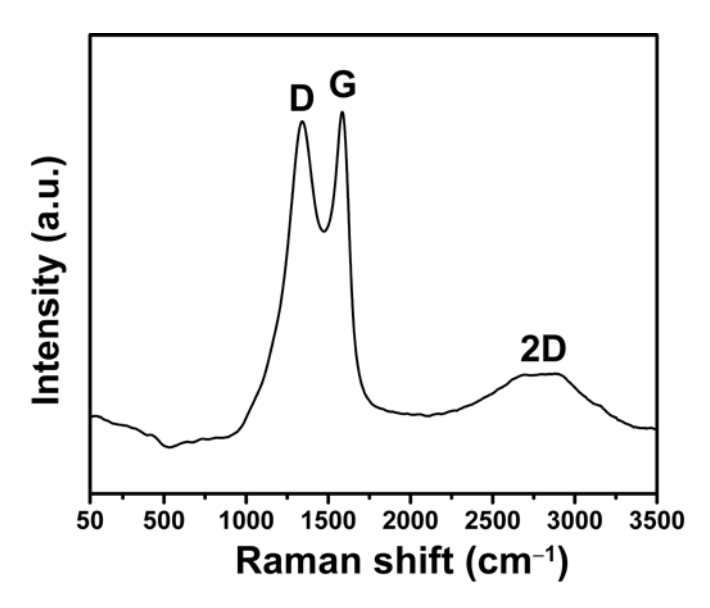


Fig. S8. Raman spectrum of carbonized cellulose fibers produced by plasma pyrolysis (pCMF).

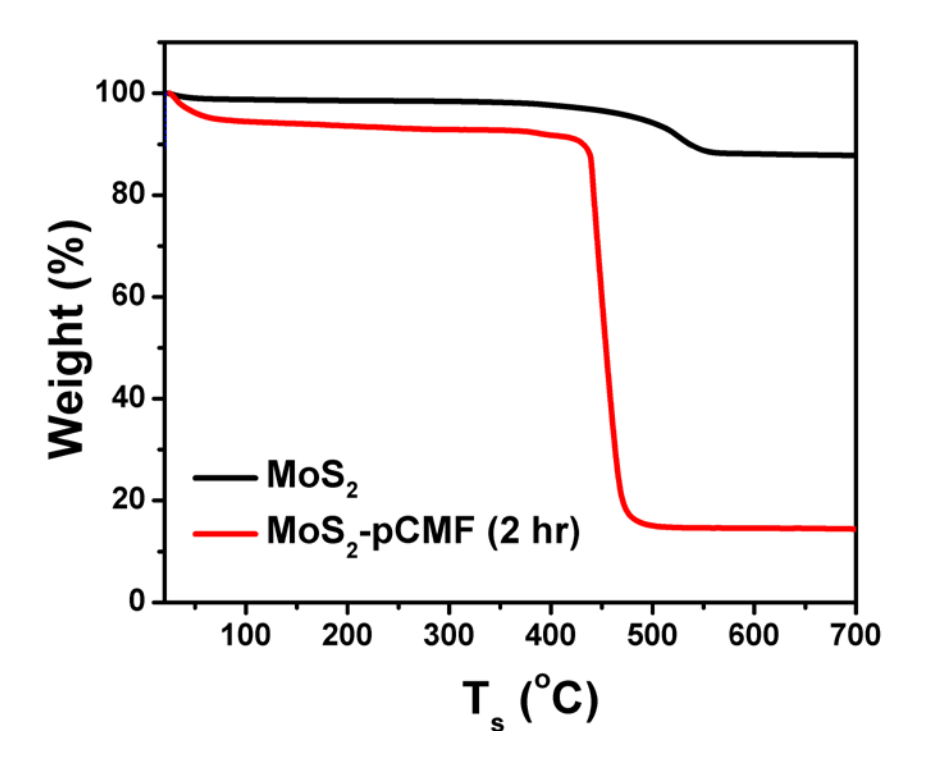


Fig. S9. TGA results of MoS₂ and MoS₂-pCMF with 2 hour growth duration.

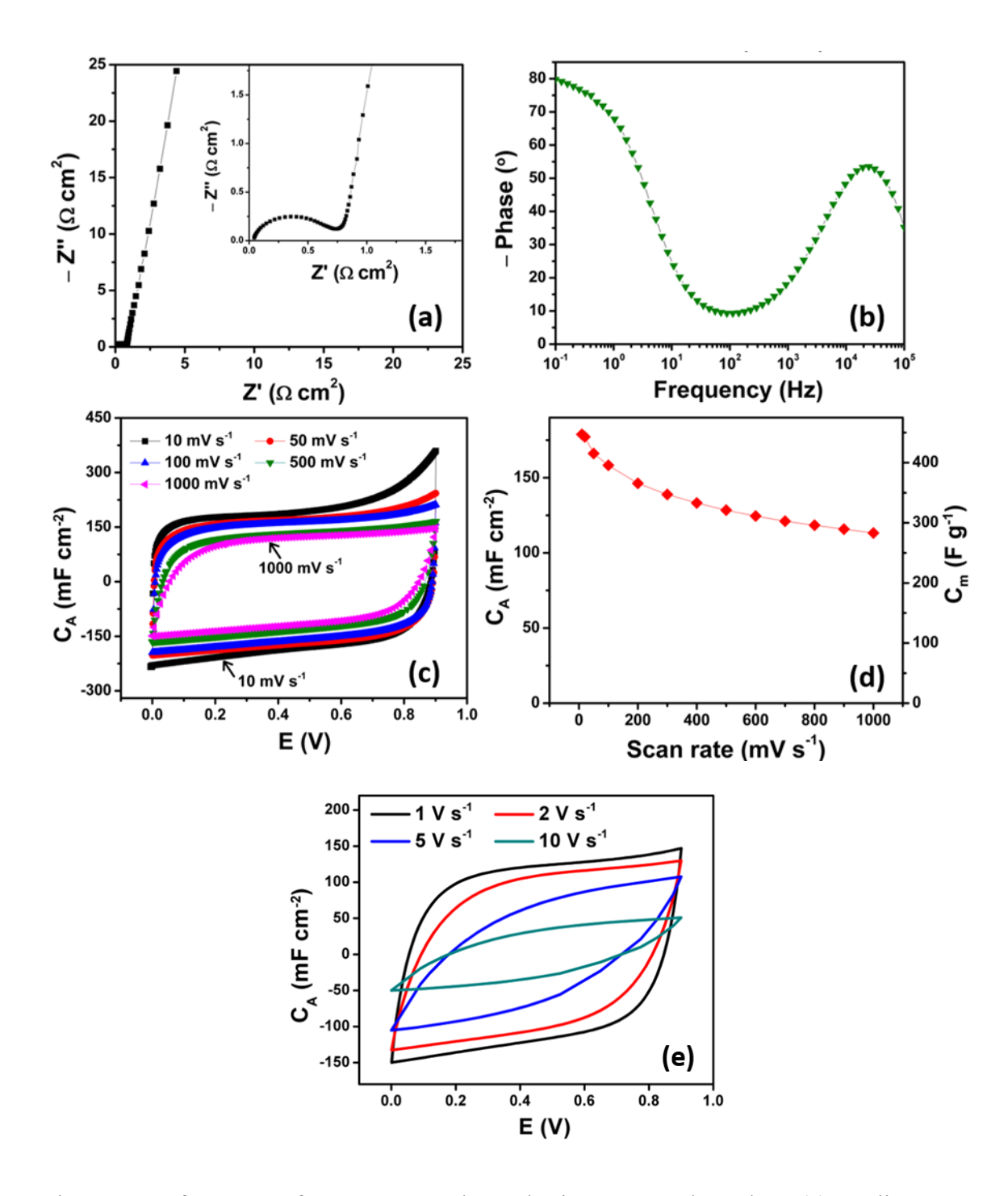


Fig. S10. Performance of MoS₂-aCMF electrodes in aqueous electrolyte. (a) Cyclic voltammetry curves. (b) Specific capacitance density versus scan rate. (c) Nyquist impedance curve. (d) Bode phase spectrum. (e) CV curves at high scan rates.

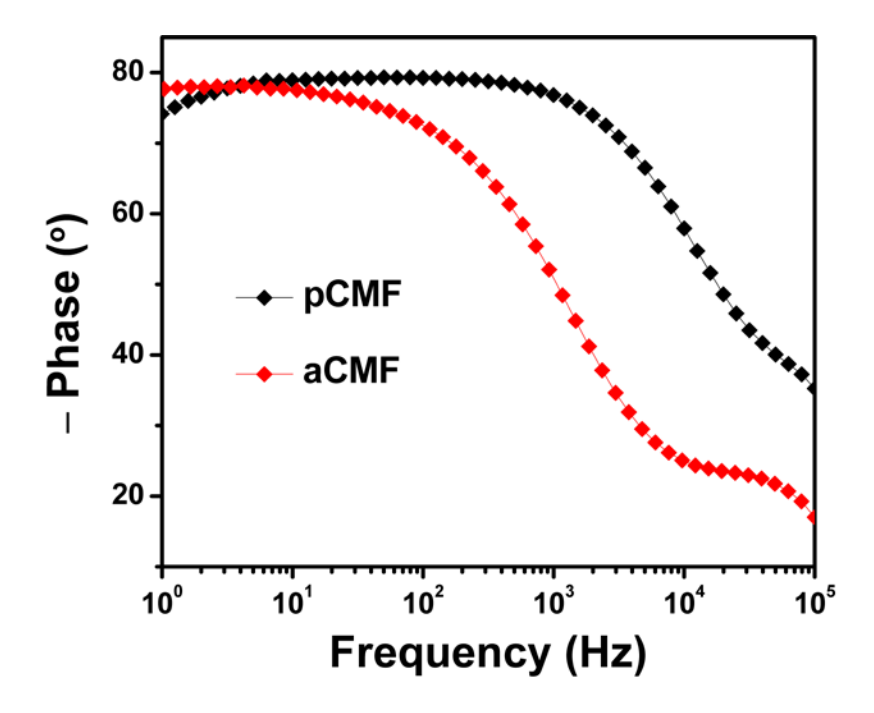


Fig. S11. Bode phase spectra of aCMF and pCMF, showing superior speed response of pCMF.

The impedance spectroscopic analysis on the 4 hours duration product is presented in Fig. S12 for comparison. A much larger semicircle is observed with knee frequency of 283 Hz (Fig. S12 (a)) and a cutoff was observed at 35 Hz (Fig. S12 (b)). As apparent from Fig. S3, the longer growth duration results into formation of flower like clusters, rather than individual sheets directly grown on the fiber surface, which will partially affect electronic conduction. The ionic motions are also relatively restricted in such clusters. The capacitance density is increased by nearly 70%, as expected from greater mass loading (Fig. S12 (c-f)). At low scan rate of 10 mV s⁻¹, the capacitance density is 176 mF cm⁻², but dramatically drops at higher scan rates.

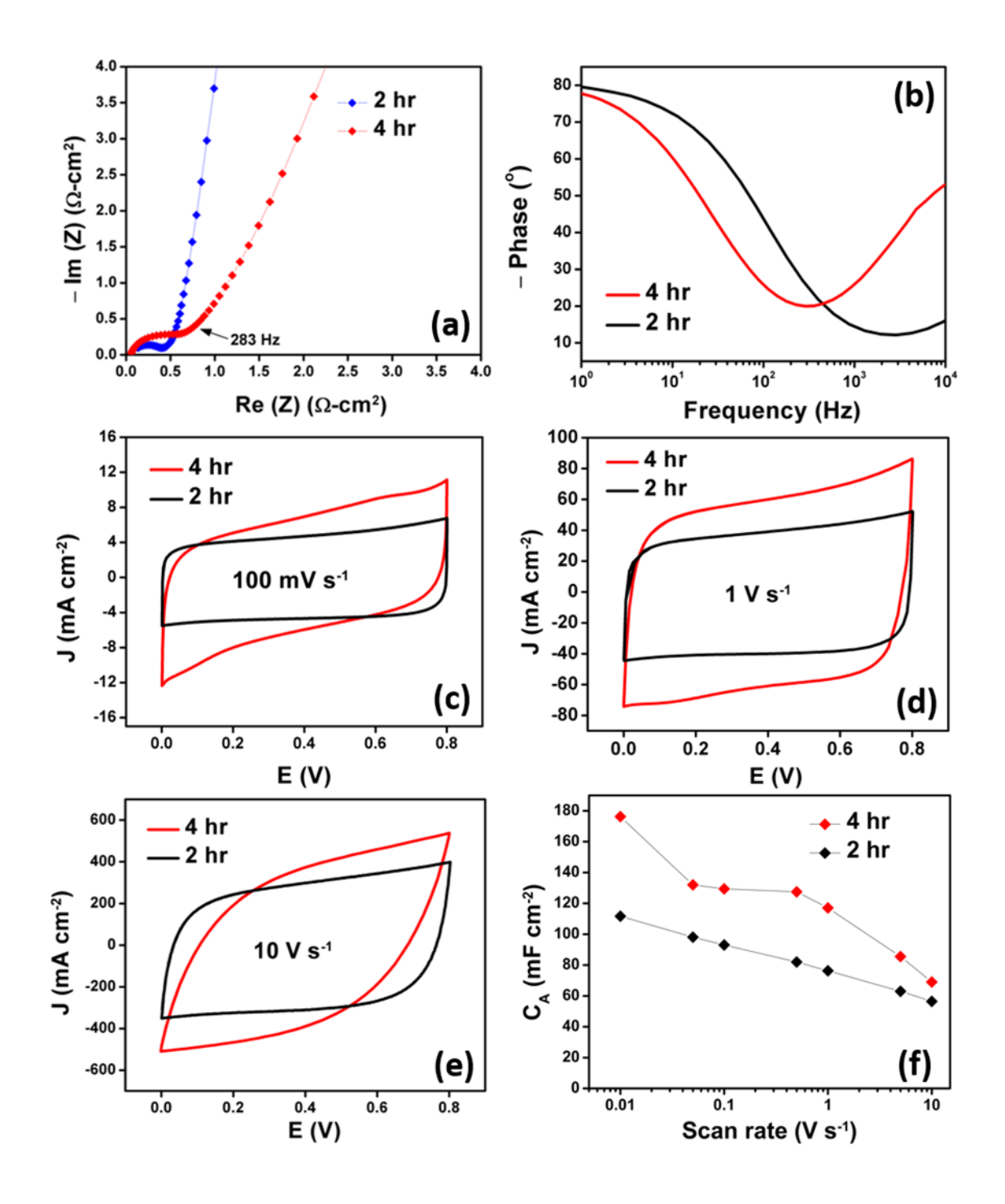


Fig. S12. Comparison of electrochemical performances of MoS2-pCMF electrodes made from 2 hours and 4 hours durations. (a) Nyquist impedance spectra. (b) Bode phase spectra. (c-e) CV scans at different scan rates. (f) Capacitance versus scan rate data for 2 and 4 hours growth durations.

The areal specific capacitance of a single electrode was calculated from cyclic voltammetry data using the following equation:

$$C_A = 2 \int I(v) dv / (V \cdot A \cdot sr)$$

where V is the voltage window, A is the area of a single electrode, and sr is the scan rate.

Energy (E) and power (P) densities of two electrode cell based on the cyclic voltammetry data were calculated for aqueous and organic electrolyte based capacitors using the following equations:

$$E = \frac{\frac{1}{8} C V^2}{3600},$$

$$P = \frac{E \times 3600}{\Delta t}$$

where C is the volumetric capacitance density of a single electrode obtained from CV measurement, V is the scan voltage window, and Δt is the time to scan between the two potential limits (from 0 to V) which is derived from the scan rate.

Power densities at different frequencies were calculated using a formula $\frac{1}{8}$ CV^2 , where C is the volumetric specific capacitance of an electrode obtained from frequency dependent impedance, *i.e.*

$$C = 2/(2 \cdot \pi \cdot f \cdot |Im(Z)| \cdot V_{\varrho})$$

V is the potential window of the respective cell and V_e is the volume of a single electrode.